

# Mechanistic Insight by *in Situ* FTIR for the Gas Phase Photo-oxidation of Ethylene by V-Doped Titania and Nano Titania

K. Bhattacharyya, S. Varma, A. K. Tripathi, S. R. Bharadwaj, and A. K. Tyagi\*

Chemistry Division, Bhabha Atomic Research Centre, Mumbai-400 085, India

Received: November 25, 2008; Revised Manuscript Received: February 2, 2009

Vanadium-doped titania is found to be a better photocatalyst for gas phase photo-oxidation of ethylene than nano titania. *In situ* FTIR studies were undertaken to elucidate the mechanistic pathway for ethylene oxidation on these two catalyst surfaces. Vanadium doping leads to formation of more chemisorbed hydroxyl species, which makes it a better photocatalyst. The labile hydroxyls which were responsible for the reduction of  $V^{5+}$  to  $V^{4+}$  during the process of calcination were also ascertained. The ethylene decomposition occurs via formation of ethoxy groups, transformed to acetaldehyde or enolates, subsequently to acetates/formates, and then to  $CO_2$ . The enolates were more stabilized on the  $TiO_2$  surface, leading to formation of formates along with the acetates. On vanadium-doped  $TiO_2$ , acetaldehyde was more stabilized than its enol tautomer, leading to the formation of labile acetic acid and acetates. The formation of the labile acetic acid, adsorbed acetates, and the adsorbed acetate  $-M$  salts led to easier oxidation of them to provide higher yield of  $CO_2$ . The higher positive charge density over Ti in  $Ti_{0.95}V_{0.05}O_2$  with respect to nano  $TiO_2$  makes the acetate (stronger nucleophile) a more stable intermediate on it.

## 1. Introduction

Titania ( $TiO_2$ ) photocatalyst has been extensively used for abatement of a wide range of contaminants, of both gaseous and aqueous nature.<sup>1–3</sup> However, it suffers from poor absorption in the visible region, rendering its use to be limited to the UV region of the electromagnetic spectrum. To extend its usefulness in the visible region of the solar spectrum, titania has been modified by both metallic and nonmetallic dopants such as transition metals and N, S, C, etc. Various methods reported for preparation of modified titania include sol–gel, coprecipitation, and ion implantation.<sup>4</sup> Anpo et al.<sup>5</sup> reported shifting of the absorption edge to the visible region by doping of titania films with 3-d transition metals, such as V, Cr, and Ni, using an ion implantation technique. A gradual red-shift in the absorption profile with increasing extent of vanadium doping has also been reported by Zhao et al. for  $V/TiO_2$  films.<sup>6</sup> A series of transition metals have been incorporated in  $TiO_2$  and tested for photocatalytic reaction under visible light by Choi et al. The effect of metal ion doping in quantum sized  $TiO_2$  particles on the photocatalytic reactivity has been discussed in detail.<sup>7,8</sup> Among all the transition metals, doping by V, Mo, and Fe exhibited maximum enhancement in the photocatalytic activity in the visible region. Doped vanadia can play multiple roles, ranging from a decrease in band gap to efficient transfer of electrons due to its multiple oxidation states ranging from 3+ to 5+ and generation of nonstoichiometry due to incorporation of  $V^{5+}$  in place of  $Ti^{4+}$ .

Mori et al.<sup>9</sup> found titania-supported vanadia to be more active than pure  $V_2O_5$  for ethylene oxidation, but they did not observe any partially oxidized products such as aldehyde. Studies on thermal oxidation of olefins over  $V_2O_5$  dispersed titania catalyst were utilized by Busca et al. to discern the effects of adsorption.<sup>10,11</sup> Apart from the fact that the selective oxidation of toluene,<sup>12</sup> benzene,<sup>13</sup> butadiene,<sup>14</sup> methanol,<sup>15</sup> and other

aliphatic alcohols<sup>16</sup> was reported on the vanadia–titania surface, it has been proven that vanadia dispersed on titania provides active sites for preferentially selective oxidation for the toluene, benzene, butadiene, etc. but lacks high selectivity for the alkenes. On the other hand, Hoffmann et al.<sup>17</sup> observed reduction in photocatalytic activity after doping of titania with vanadium for photooxidation of 4-chlorophenol. Thus, the exact role of V-doping in enhancement of photocatalytic activity of  $TiO_2$  still needs to be established.

IR studies on heterogeneous catalytic oxidation of olefins on vanadia–titania systems have been reported at elevated temperatures,<sup>18</sup> and very few of them deal with photocatalytic oxidation of ethylene under ambient conditions.<sup>19</sup> For example, Busca et al. in IR studies on heterogeneous catalytic oxidation of ethylene over vanadia–titania catalyst have reported that reactive adsorption of ethylene starts from 373 K and results in the formation of acetaldehyde, acetates, and formate species upon heating.<sup>12</sup> Formation of similar formate and acetate species was observed by us during photocatalytic oxidation of ethylene at room temperature over uranyl-incorporated MCM-41 catalyst.<sup>19</sup>

Recently we have reported the synthesis of single phasic nanosized ( $\sim 12$  nm) V-doped (up to 10 mol %) titania using a modified sol–gel route.<sup>20</sup> The photocatalytic activity of this material was evaluated for oxidation of ethylene in air at room temperature under sunlight type irradiation, where the role of the oxidation state of vanadium in maximizing the photocatalytic activity of the V-doped sample was convincingly established.

The consequences of vanadium being doped in the crystal lattice rather than being dispersed in the titania surface for the ethylene oxidation and also knowing the intermediates produced in the course of the reaction have yet to be verified. Present work thus deals with *in situ* IR experiments carried out under UV–visible irradiation conditions at room temperature and is aimed to delineate the role of vanadium doping in enhancement of the photocatalytic activity of doped titania for photocatalytic oxidation of ethylene in air. An attempt is also made to

\* To whom correspondence should be addressed. E-mail: aktyagi@barc.gov.in. Phone: +91-22-25595330. Fax: +91-22-25505151.

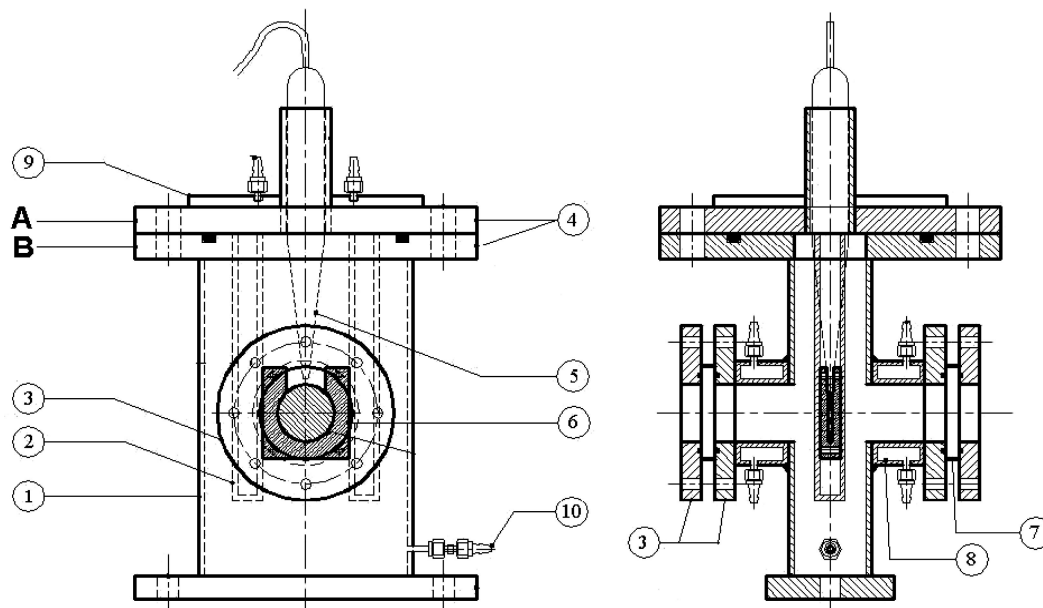


**Figure 1.** Front and side view of a stainless steel cell for the *in situ* FTIR study of a catalyst surface during photocatalytic reactions. (A) Top flange with a sample heater block and a UV lamp. (B) cell body: (1) rectangular stainless steel body; (2) cartridge heater block; (3) and (4) flanges; (5) UV pen-ray lamp/visible lamp; (6) sample holder block; (7)  $\text{CaF}_2$  window; (8) and (9) cooling water jackets; and (10) manifold with gas inlet/outlet and evacuation facility.

emphasize the role of various surface transient species in the photooxidation process and to understand the role of a doped metal, on the stabilization of the intermediates on the surface. To the best of our knowledge, this is the first work of its kind on the V-doped  $\text{TiO}_2$  samples using *in situ* FTIR spectroscopy to investigate the surface species involved in the vapor phase photocatalytic oxidation of ethylene under *in situ* UV/visible irradiation at ambient conditions.

## 2. Experimental Section

**2.1. Synthesis and Characterization.** A simple new method was used for the preparation of the nano titania and 5 mol % vanadia-doped titania. In this sol-gel process ammonium metavanadate was initially dissolved in water at room temperature at a neutral pH in the required stoichiometric amount without using any buffer solution. The solution of meta-vanadate was maintained at  $0^\circ\text{C}$  by the addition of an ice-salt mixture from outside. To this dissolved meta-vanadate solution was added dropwise with vigorous stirring for 1 h a  $\text{Ti(IV)}$  isopropoxide solution in isopropanol, resulting in the formation of a consistent gel. This gel was then stirred for another 1 h. The gel was kept for nucleation for 12 h in the dark and then dried at room temperature for 12 h. The mass was then dried in an oven at  $100^\circ\text{C}$  for 4 h. The resulting solid mass was crushed and calcined at a temperature of  $500^\circ\text{C}$  for 4 h. Samples with 5.0 mol % of V doping were prepared by mixing a stoichiometric amount of ammonium metavanadate solution in water with  $\text{Ti(IV)}$  isopropoxide. Equivalently, the nano titania was prepared by not adding any meta-vanadate solution.

The powder X-ray diffraction patterns were collected on a Philips analytical diffractometer (using Ni-filtered  $\text{Cu K}\alpha$  radiation). The average crystallite size of anatase phases was determined according to the Scherer equation. Laser Raman spectra were taken on a LABRAM-1 spectrometer (backscattering geometry, excitation source  $\text{Ar}^+$  ion laser, spectral resolution of  $2\text{ cm}^{-1}$ ). An electron paramagnetic resonance

(EPR) study was carried out using a BRUKER, EMX EPR spectrometer with a microwave frequency of 9.34 GHz. EPR spectra were taken both at liquid nitrogen temperature (77 K) and at room temperature. The recording parameters were 3365 G central field, 1.0 G modulation amplitude, 100 kHz modulation frequency, and 41.04 s sweep time. All the spectra were recorded at the microwave power 6.34 mW (attenuation 15 dB).

**2.2. Activity Measurement.** The activity measurements were carried out at room temperature in a 40 mL capacity cylindrical quartz/Pyrex reactors of 20 mm diameter, placed horizontally in a chamber close to a water-cooled medium pressure mercury vapor lamp (400 W). The said lamp exhibits very broad range emission spectra having maxima at both UV and the visible range, with the UV-part being only 16% of the whole spectra. The catalytic activity experiments were conducted in static mode for a (1–5 mol %) ethylene in air mixture, in the presence of a well-dispersed 100 mg of catalyst. The overall pressure in the reaction cell was  $\sim 1.5$  atm. After insertion of the ethene and the air mixture to the evacuated catalyst present in the above-described reactor in vacuum, they were left under ambient conditions for 15 min to attain the adsorption equilibrium. The reaction products were analyzed over a period of about 3–5 h, at 30–45 min intervals. A gas chromatograph (CIC GC-2011, India), equipped with a Porapak-Q (2 m length) column and with thermal conductivity and flame ionization detectors, was employed in isothermal temperature mode at a  $100^\circ\text{C}$  oven temperature. Identical experiments were also carried out with anatase titania (Aldrich, purity  $\geq 99\%$ ) for comparison.

**2.3. In Situ FTIR.** *In situ* FTIR studies were performed in transmission mode on a JASCO 610 spectrophotometer, using an indigenously developed cell equipped with two water cooled  $\text{CaF}_2$  windows and fitted with either a low pressure mercury discharge lamp (Pen-Ray lamp, UVP 11SC-1, USA, operating at 5.5 W) as a UV source or a tungsten-halogen lamp (12 V, 35 W) as a visible light source. A schematic of this cell is presented in Figure 1. The Pen ray source has 92% emission at 253.7 nm, with the remaining

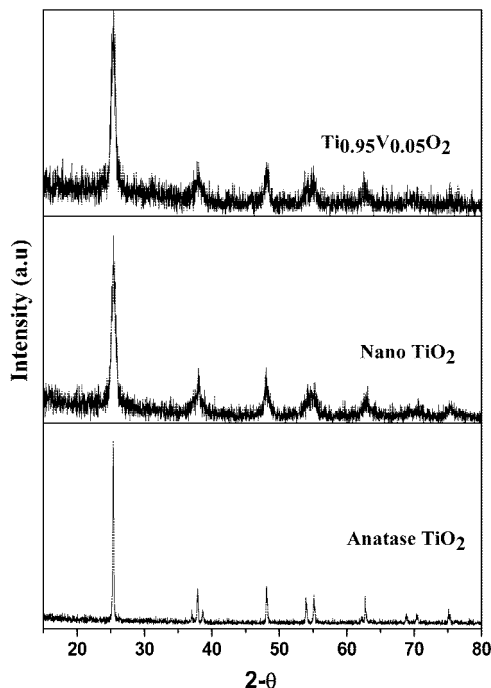


**Figure 2.** XRD patterns of nano titania and vanadia-doped titania samples along with bulk anatase titania.

emission being in the form of spectral lines in the 295 to 365 nm region. The intensity of this lamp for the 253.7 nm line is rated at  $42 \text{ W cm}^{-2}$ . The light from this lamp was focused vertically over the catalyst wafer, and because of its being a low intensity source, there was no rise in sample temperature during irradiation. A self-supported sample wafer (25 mm diameter, 0.8 mm thickness, weight  $\sim 80 \text{ mg}$ ) was employed for this purpose. Prior to dosing with an ethylene–air mixture (6.6 vol %), the sample wafer were subjected to overnight degassing at 573 K for the removal of any adsorbed species such as moisture, etc. Normally, 300 scans were coadded, and the spectra were recorded by using a similarly treated but unexposed pellet as background. Identical experiments were also performed on nano titania to delineate the role of V-doping in titania during photocatalytic oxidation of ethylene. Unless mentioned otherwise, the gas phase contribution from ethylene has been properly subtracted in IR spectra presented in this study.

### 3. Result and Discussion

**3.1. XRD.** Figure 2 shows the characteristics of the XRD peaks of different titania- and vanadia-doped samples. The XRD patterns of nano titania and the other catalyst samples show peaks at  $2\theta = 25.4^\circ, 38.1^\circ, 48.0^\circ, 54.9^\circ, 62.8^\circ,$  and  $75.1^\circ$ , which are the signature peaks of the anatase titania. The XRD pattern corresponding to nano titania is found to match with that of the anatase phase (JCPDS 21-1272). The nano titania on calcining at 500 °C for 4 h has no rutile phase and is completely anatase in nature. In the XRD pattern of the vanadia-doped titania sample, there are no characteristic peaks of either vanadium oxides or any other phases, implying that they are single phasic with the titania anatase type phase. Thus, it can be inferred that either the vanadium ions are substituted into the crystal lattice sites of the titania or present as highly dispersed vanadium oxide on the titania surface. The vanadium-doped and undoped nano titania exhibited Raman bands at 394, 513, and  $639 \text{ cm}^{-1}$ ; this confirms the presence of only the titania anatase phase. Also, in the spectra the complete absence of the bands at 285, 703,

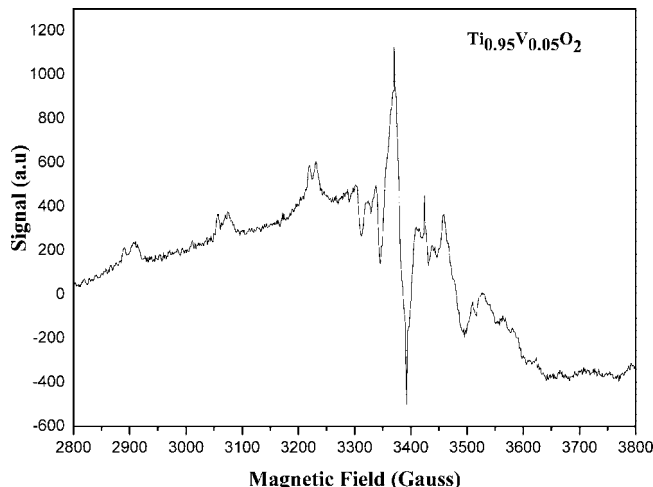


**Figure 3.** EPR profile of a vanadia-doped titania sample.

and  $997 \text{ cm}^{-1}$  indicates the absence of the crystalline  $\text{V}_2\text{O}_5$  phase. As no absorption peaks are observed at  $\sim 930$  and  $1030 \text{ cm}^{-1}$ , the presence of polymeric and monomeric surface vanadia species can also be ruled out. Our previous report can be referenced for details of the Raman data. Based on the detailed characterization of these samples,<sup>20</sup> it can now be stated that the vanadium is incorporated in the crystal lattice sites of the  $\text{TiO}_2$  and is not present as any highly dispersed separate phase of  $\text{V}_2\text{O}_5$ .

**3.2. EPR Studies.** The EPR spectrum of the vanadium-doped  $\text{TiO}_2$  sample at 77 K is shown in Figure 3. The nano  $\text{TiO}_2$  was EPR inactive, but the vanadium-doped  $\text{TiO}_2$  showed a parallel splitting of 7 and a vertical splitting of 5, which is typical of  $\text{V}^{4+}$ , which is typically the  $d^1$  state being EPR active. These results are in good agreement with the V-doped  $\text{TiO}_2$  spectra in the literature.<sup>17,21</sup> The calculated  $g$  value from the spectrum as calculated with respect to DPPH (2.0032) is 1.98, which agrees well with the literature value.<sup>17,21</sup> Thus, it can be inferred that the doped vanadium is definitely present in the +4 state rather than in the +5 state in the  $\text{TiO}_2$  lattice. The presence of  $\text{V}^{4+}$  in the V-doped  $\text{TiO}_2$  catalyst can be initiated due to the reduction of  $\text{V}^{5+}$  by  $\text{Ti}^{3+}$  generated during the calcination of the catalysts. The dehydroxylation of  $\text{Ti}^{4+}$  sites results in the formation of  $\text{Ti}^{3+}$ , which is followed by charge transfer to  $\text{V}^{5+}$ , resulting in the reduction of  $\text{V}^{5+}$  to  $\text{V}^{4+}$ , thereby forming stable linkages of  $\text{Ti}-\text{O}-\text{V}$ . A mechanism for the spontaneous reduction of  $\text{V}^{5+}$  was proposed by Trifiro<sup>22</sup> in his study of the solid-state preparation of  $\text{V}_2\text{O}_5/\text{TiO}_2$ . Herrmann et al.<sup>23</sup> also similarly proposed that vanadium may be incorporated as  $\text{V}^{4+}$  in the crystal lattice sites of  $\text{TiO}_2$  in their study of  $\text{V}_2\text{O}_5/\text{TiO}_2$  catalysts, at the calcination temperature of 450 °C. They also reported the presence of  $\text{Ti}-\text{O}-\text{V}$  linkages, comparable with the findings of Trifiro. Both the above-mentioned studies substantiated the reduction of  $\text{V}^{5+}$  to  $\text{V}^{4+}$ , as also observed by us in our V-doped  $\text{TiO}_2$  photocatalyst. A high concentration of hydroxyl groups is always present in the  $\text{TiO}_2$  surface, and subsequent calcination will lead to the formation of  $\text{Ti}^{3+}$  and consequently the formation of the  $\text{V}^{4+}$ , as in our case also, where the calcination was performed at 500 °C. In addition detailed studies on the XPS were also reported in our previous report.<sup>20</sup> It was found from the XPS studies that the V is present in both  $\text{V}^{4+}$  and  $\text{V}^{5+}$  oxidation states in the V-doped titania samples. The ratio of  $\text{V}^{4+}$  to  $\text{V}^{5+}$  was highest and optimum in the  $\text{Ti}_{0.95}\text{V}_{0.05}\text{O}_2$  photocatalyst. For the nano



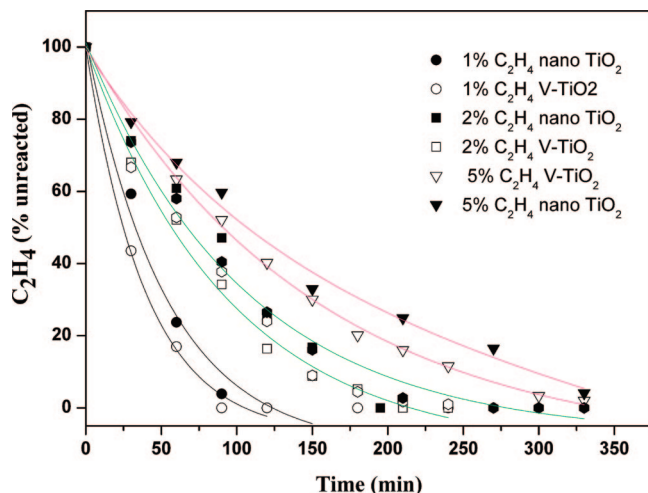


**Figure 4.** Photocatalytic degradation of ethylene for the percent of unreacted  $C_2H_4$  left with time for different concentrations of an ethylene air mixture on the V-doped  $TiO_2$  and anatase  $TiO_2$ .

**TABLE 1:  $t_{1/2}$  Values for V-Doped Titania and Nano Titania as a Function of Ethylene Air Ratio**

ethylene conc	$t_{1/2}$ of the nano $TiO_2$ system	$t_{1/2}$ of $Ti_{0.95}V_{0.05}O_2$
1mol%	39	28
2mol%	76	65
5mol%	115	95

titania,  $Ti\ 2p_{3/2}$  and  $Ti\ 2p_{1/2}$  peaks are observed at 458.5 and 464.06 eV, respectively, and that for the  $Ti_{0.95}V_{0.05}O_2$  shows a shift toward higher binding energy values by  $\sim 0.9$  eV. Thereby with the vanadium doping in the  $TiO_2$  crystal lattice sites, the binding energy increment can be attributed to conversion of the  $Ti^{4+}$  to  $Ti^{(4+\delta)}$ .<sup>20</sup>

**3.3. Photocatalytic Degradation of Ethylene on the V-Doped  $TiO_2$  and the Pristine  $TiO_2$ .** Figure 4 depicts the photocatalytic oxidation of ethylene under ambient conditions, with different concentrations of the reactant ethylene molecule. Figure 4 represents the unreacted ethylene left after oxidation against time by the nano titania and the  $Ti_{0.95}V_{0.05}O_2$  catalysts for different concentrations of  $C_2H_4$  and air mixtures, viz. of 1 mol %, 2 mol %, and 5 mol % ( $C_2H_4$  + air mixture). The  $Ti_{0.95}V_{0.05}O_2$  sample showed the maximum photocatalytic activity among all the different V-doped titania samples (1–10 mol %) and nano titania as reported in our earlier publication.<sup>20</sup> Also there is a steady decrease in the band gap as a function of vanadium doping in the  $TiO_2$  lattice sites which varies from 3.24 eV for pristine anatase titania to 2.31 eV for a sample doped with 10 mol % vanadium.<sup>20</sup> Therefore, in our present work this sample along with the nano titania was tacitly chosen to probe the reaction pathway for the ethene photooxidation using *in situ* FTIR as a probe. It was found that, at low concentration of  $C_2H_4$ , complete mineralization occurs in a shorter time. Irrespective of the concentration of ethylene, it is quite definite that the  $Ti_{0.95}V_{0.05}O_2$  titania is more active and shows higher  $CO_2$  formation than the nano titania. The reaction rate also becomes slower as we go toward higher concentrations of  $C_2H_4$ . This can be ascertained from the increasing  $t_{1/2}$  value as a function of  $C_2H_4$  concentration. The respective  $t_{1/2}$  value for V-doped  $TiO_2$  and that of nano  $TiO_2$  are as given in Table 1. This trend may be due to the fact that oxygen in air may be playing a significant role. For the photocatalytic activity we get only  $CO_2$  and  $H_2O$  as the final product in the GC, as no other

partial oxidation products were detected in the FID. The catalysts were used for four to five cycles of reaction with a pretreatment of the catalyst after reaction to a temperature of 100 °C. The structural stability of the catalyst was found to be intact after five cycles of reaction.

**3.4. FT-IR Spectroscopy Results. (a) Adsorption of Ethylene over Nano  $TiO_2$  and V-Doped  $TiO_2$ .** Figure 5 shows the IR spectra for adsorption of an ethylene–air mixture (1:14) over nano titania (curve b) and V-doped titania (curve c) under ambient temperature and pressure conditions. Curves d and e show corresponding difference spectra obtained by appropriate subtraction of the gaseous ethylene spectrum (curve a), whose respective bands are ascribed in Table 2.<sup>24,25</sup> A comparison of the spectra shown in curves a, b, and c reveals the presence of IR bands similar to those of gaseous ethylene while they are absent in the difference spectra (curve d and e), suggesting weak adsorption of ethylene on both nano titania and V-doped titania surfaces. In addition, negative bands in the  $\nu(OH)$  region, a broad band in the 3600–3000  $cm^{-1}$  region, and the appearance of several new bands in the 1700–1150  $cm^{-1}$  region can be seen in the difference spectra. The nature of these bands depended on the sample used. Thus, on a nano titania surface, negative bands at 3715 and 3663  $cm^{-1}$  and the appearance of a broad band in the 3600–3000  $cm^{-1}$  region revealed the interaction of ethylene with the surface hydroxyl groups and formation of hydrogen bonding, and it is the isolated hydroxyl group (3715  $cm^{-1}$ ) that has shown higher reactivity toward ethylene (Figure 5, curve d). On the other hand, hydroxyl groups associated with vanadium in V-doped titania interacted predominantly with the ethylene, as suggested by the appearance of the negative IR band at 3657  $cm^{-1}$  (Figure 5, curve e). The spectral features in the lower frequency region (2000–1150  $cm^{-1}$ ) are different on both samples, as is seen by the presence of several absorption bands at 1630, 1550, 1420, 1320, and 1186  $cm^{-1}$  on nano titania (Figure 5, curve d) compared to only one band at 1622  $cm^{-1}$  on V-doped titania (Figure 5, curve e). IR bands at  $\sim 1630$  and 1320  $cm^{-1}$  have been associated with the  $C=C$  stretching and  $CH_2$  symmetric scissoring vibrations of adsorbed ethylene molecules which otherwise are IR forbidden (Raman active) in the gas phase.<sup>26</sup> Adsorption of ethylene is suggested to take place via interaction of  $\pi$ -electrons with the cationic sites on both  $TiO_2$  and V-doped  $TiO_2$  samples, and as a result the  $D_{2h}$  symmetry of free ethylene is lowered. A closer look at the IR band at  $\sim 1630$   $cm^{-1}$  observed on nano titania reveals that it is broader compared to that observed at 1624  $cm^{-1}$  on V-doped  $TiO_2$  and on deconvolution (not shown here) shows a clear shoulder at  $\sim 1618$   $cm^{-1}$ . Absorption bands at 1630, 1618, and 1186  $cm^{-1}$  are reported for the enolic form ( $CH_2=CHO-$ ) of acetaldehyde.<sup>27</sup> It is known that acetaldehyde is produced by dehydrogenation of ethoxy species, which in turn are generated on the surface during interaction of ethylene with surface hydroxyl groups. In fact, in vinyl ethers it has been shown that the  $\nu(C=C)$  band is split due to a Fermi resonance with the first overtone of the  $>CH_2$  wagging node.<sup>28,29</sup> A weak band at 1186  $cm^{-1}$  could be due to the  $\nu(C-O)$  of this species. An alternative possible assignment for these bands is to the crotonic condensation product crotonaldehyde. With these observations, it can be inferred that the adsorption of ethylene is stronger on the nano  $TiO_2$  sites than that on the V-doped surface and leads to formation of  $CH_2=CH_2-O-$  type species.

At this moment assignment of a broad peak at 1550  $cm^{-1}$  observed only on the nano titania surface (Figure 5 curve d) is difficult; however, occurrence of such a peak has been reported earlier on the  $Fe_2O_3$  and the  $Co_3O_4$  surfaces and is assigned to

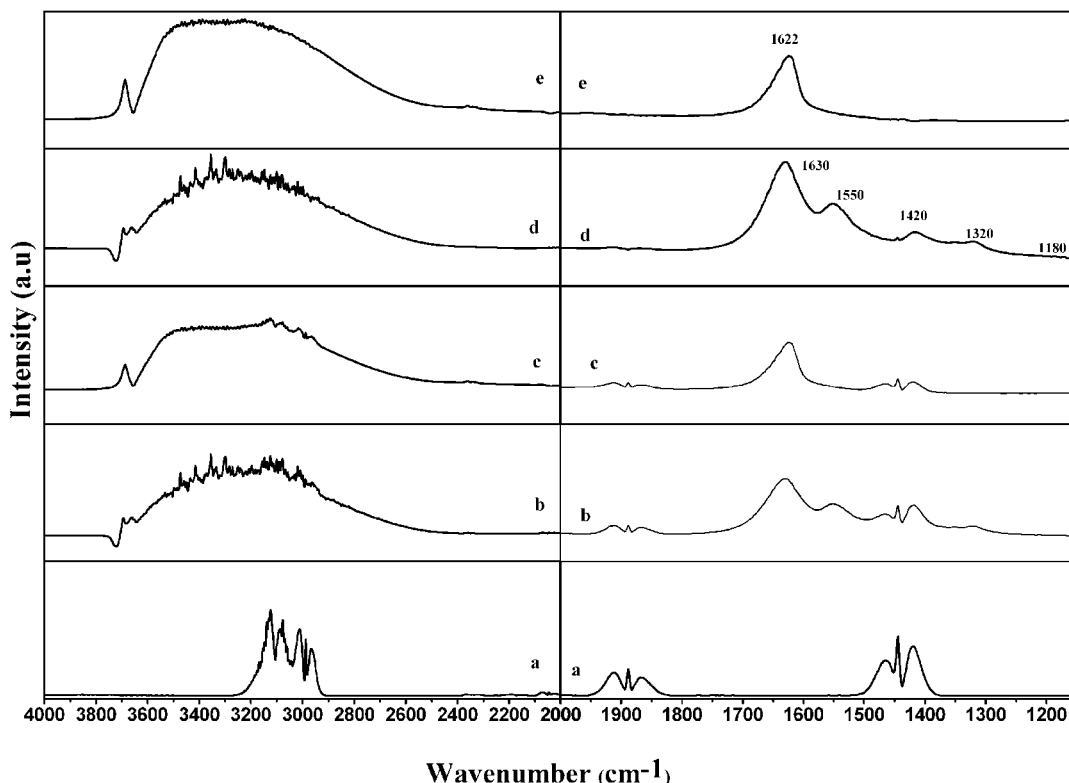


**Figure 5.** *In situ* FTIR spectra of (a) gaseous ethylene without any air, (b) an adsorbed ethylene and air mixture after 30 min on a nano TiO<sub>2</sub> surface without subtraction of the ethylene spectra, (c) an adsorbed ethylene and air mixture after 30 min on a V-doped TiO<sub>2</sub> surface without subtraction of the ethylene spectra, (d) an adsorbed ethylene and air mixture after 30 min on a nano TiO<sub>2</sub> surface after subtraction of the ethylene spectra, and (e) an adsorbed ethylene and air mixture after 30 min on a V-doped TiO<sub>2</sub> surface after subtraction of the ethylene spectra.

**TABLE 2: Observed Wave Numbers and Assignments of Gaseous Ethylene**

vibration	assignment	symmetry	IR gas phase ethene (IR active) (cm <sup>-1</sup> ) <sup>a</sup>	IR gas phase ethene (IR inactive) (cm <sup>-1</sup> ) <sup>b</sup>	on TiO <sub>2</sub> surface <sup>c</sup>	on V-TiO <sub>2</sub> surface
$\nu_9$	$\nu_a\text{CH}_2$	$B_{2u}$	3105		3129 <sup>c</sup>	3129 <sup>c</sup>
$\nu_5$	$\nu_a\text{CH}_2$	$B_{1g}$		3083	3080 <sup>d</sup>	3080 <sup>d</sup>
$\nu_2 + \nu_{12}$	$(\nu_a\text{C}=\text{C}) + (\delta\text{CH}_2)$	$B_{3u}$	3067		3060 (very strong) <sup>c</sup>	3060 (weak) <sup>c</sup>
$\nu_1$	$\nu_s\text{CH}_3$	$A_g$		3021	3019 <sup>d</sup>	3016 <sup>d</sup>
$\nu_{11}$	$\nu_s\text{CH}_2$	$B_{2u}$	2989		2985 <sup>c</sup>	2983 <sup>c</sup>
$\nu_7 + \nu_8$	$2\omega\text{CH}_2$	$B_{3u}$	1888		1889 <sup>c</sup>	1889 <sup>c</sup>
$\nu_2$	$\nu\text{C}=\text{C}$	$A_g$		1625	1632 <sup>d</sup>	1620 <sup>d</sup>
$\nu_{12}$	$(\delta\text{CH}_2)$	$B_{3u}$	1443		1445 <sup>c</sup>	1445 <sup>c</sup>
$\nu_3$	$(\delta\text{CH}_2)$	$A_g$		1343	1345 <sup>d</sup>	
$\nu_4$	$\text{tCH}_2$	$A_u$	1023			
$\nu_7$	$\text{wCH}_2$	$B_{1u}$	949			
$\nu_8$	$\text{wCH}_2$	$B_{2g}$		943		
$\nu_{10}$	$\text{rCH}_2$	$B_{2u}$	826			

<sup>a</sup> These are observed in Figure 5a: refs 26 and 27. <sup>b</sup> These are Raman active bands: ref 28. <sup>c</sup> Observed in both Figure 5b and c. <sup>d</sup> Observed in Figure 5d and e. <sup>e</sup> Apart from these there is a peak at 1550 cm<sup>-1</sup> on nano TiO<sub>2</sub>.

the IR-activated  $\nu_2$  (C=C stretching) vibration of ethylene.<sup>30,31</sup> Thus, the IR band at 1550 cm<sup>-1</sup> might be assigned to this vibration arising due to interaction of ethylene with the inherent defect sites present on the nano titania sample.

Figure 6 represents the deconvolution of the broadband produced in the hydroxyl region for both nano titania and V-doped titania into two peaks with maxima at 3410 and 3120 cm<sup>-1</sup>. Deconvolution of this broad peak was carried out employing the Gaussian model for multiple peaks fitting after the baseline correction. Fitting results of  $\chi^2$  values of 0.081 and 0.075 were obtained respectively for the (a) nano TiO<sub>2</sub> and the (b) V-doped TiO<sub>2</sub>. Bezrodna et al.<sup>32,33</sup> have shown that at least two types of energy nonequivalent active centers can be distinguished on the TiO<sub>2</sub> surface. The first band at ~3411 cm<sup>-1</sup>

corresponds to the “weak” surface active sites, on which physisorbed water-like (H<sub>2</sub>O)<sub>n</sub> molecules are bound by hydrogen bonds, with each other and with the OH-groups of the TiO<sub>2</sub> surface. The other band at ~3200 cm<sup>-1</sup> is attributed to the water complexes or the chemisorbed water molecules, strongly bound with the TiO<sub>2</sub> surface like H<sub>2</sub>O...HO-Ti, {HOH...O(H)-Ti}.<sup>32,33</sup> Table 3 represents the effective ratios of these two sites. Now for the photocatalytic phenomenon the band at ~3200 cm<sup>-1</sup> becomes more important, as this site represents the chemisorbed hydroxyl intermediates which undergo a subsequent photochemical process, highlighted later in the proposed reaction mechanism. Also, the formation of the radical species in the case of strongly bound water molecules will be enhanced. It can be observed from Table 3 that for vanadium-doped TiO<sub>2</sub>

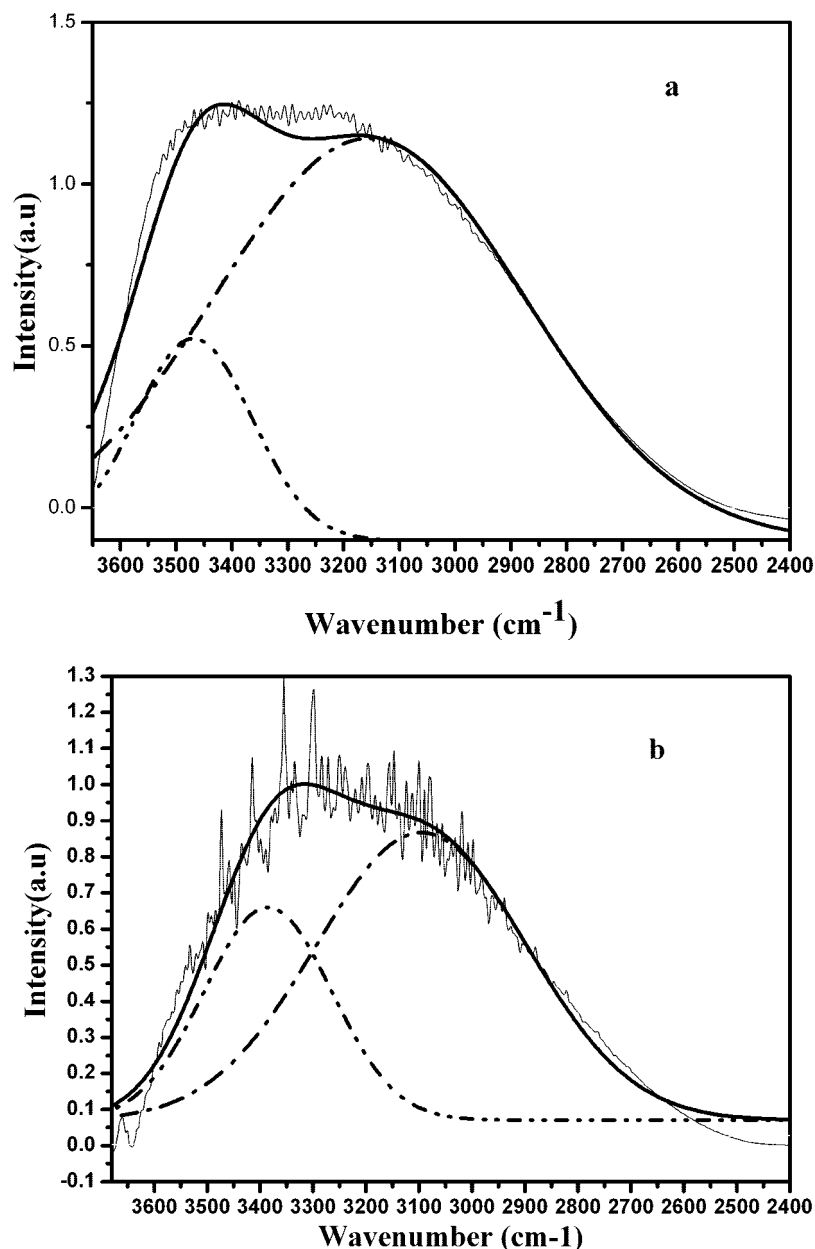


**Figure 6.** Deconvoluted fragments of the IR spectra in the region of OH-group stretching vibrations: (a) V-doped titania; (b) nano titania.

**TABLE 3: Spectral Component Parameters of the  $\nu(\text{OH})$  Absorption Band for  $\text{TiO}_2$  and V-Doped  $\text{TiO}_2$**

sample	$\nu_{\text{max}}$	area	fwhm	area ratio
nano $\text{TiO}_2$	3410	177	233	0.44
	3210	398	395	
$\text{Ti}_{0.95}\text{V}_{0.05}\text{O}_2$	3410	164	201	0.19
	3210	866	553	

the peak corresponding to the  $\sim 3200\text{ cm}^{-1}$  band shows a 2-fold enhancement. This clearly indicates increased formation of the chemisorbed hydroxyl species on this sample, thereby making it a more efficient photocatalyst.

**(b) Effects of UV-Irradiation on the Ethylene and Air Mixture Subsequent to Adsorption over Nano  $\text{TiO}_2$  and V-doped  $\text{TiO}_2$ .** Samples exposed to an ethylene–air mixture were further subjected to UV irradiation from the source, as mentioned above, and the FT-IR spectra were taken as a function of time. Difference spectra (ethylene gas phase subtracted) marked as 1 and 2 in Figures 7 and 8 show these results on V-doped  $\text{TiO}_2$  and nano  $\text{TiO}_2$  surfaces when subjected to

irradiation for up to 90 min, respectively. The intermediate species so produced in the reaction course are discussed in the following section.

The higher frequency region of  $4000\text{--}2000\text{ cm}^{-1}$  is shown for the  $\text{TiO}_2$  surface in Figure 7a. Irradiation of this sample results in the appearance of a broad band in the  $3600\text{--}2600\text{ cm}^{-1}$  region. The intensity of these bands increased with irradiation time. The broad band with a center at  $\sim 3200\text{ cm}^{-1}$  may find its origin in the  $\nu(\text{OH})$  vibrations of the carboxylic acid group or that of enolates formed during irradiation. Bands at  $2942$ ,  $2880$ , and  $2740\text{ cm}^{-1}$  have been associated with different vibrations of the formate species (described subsequently in the reaction mechanism).<sup>34</sup> The progressive growth of the IR bands centered at  $2349\text{ cm}^{-1}$  due to  $\nu_3(\text{CO}_2)$  vibrations of carbon dioxide and that at  $1630\text{ cm}^{-1}$  due to the bending vibrations of water confirms the increased yield of these products with irradiation time. In the lower frequency region (Figure 8), peaks at  $1642$  and  $1584\text{ cm}^{-1}$  along with the shoulder at  $1618\text{ cm}^{-1}$  (attributed to the  $\text{C}=\text{C}$  stretch of the enolate form) grow

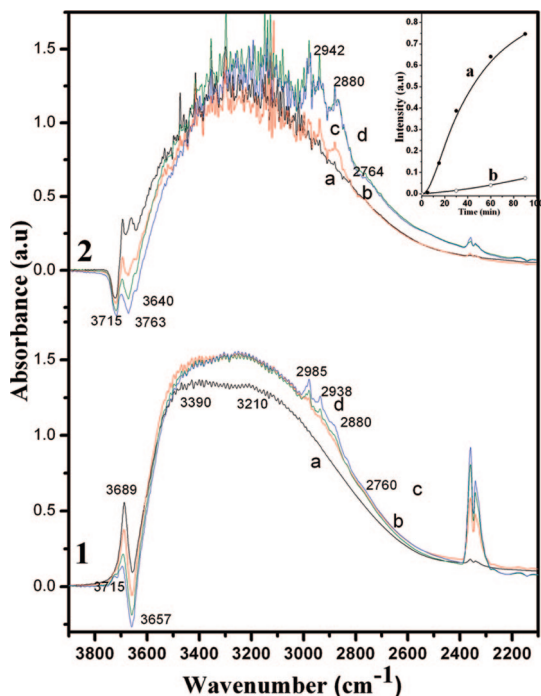


**Figure 7.** *In situ* FT-IR spectra in the (4000–2000)  $\text{cm}^{-1}$  range for (1) V-doped  $\text{TiO}_2$  and (2) nano  $\text{TiO}_2$  exposed to an ethylene–air mixture followed by *in situ* UV-irradiation for (a) 0 min, (b) 30 min, (c) 60 min, and (d) 90 min. The inset shows a comparative plot of the IR band intensity of the  $\nu_3\text{CO}_2$  peak at  $2349\text{ cm}^{-1}$  vs time for (a) V-doped  $\text{TiO}_2$  and (b) nano  $\text{TiO}_2$ .

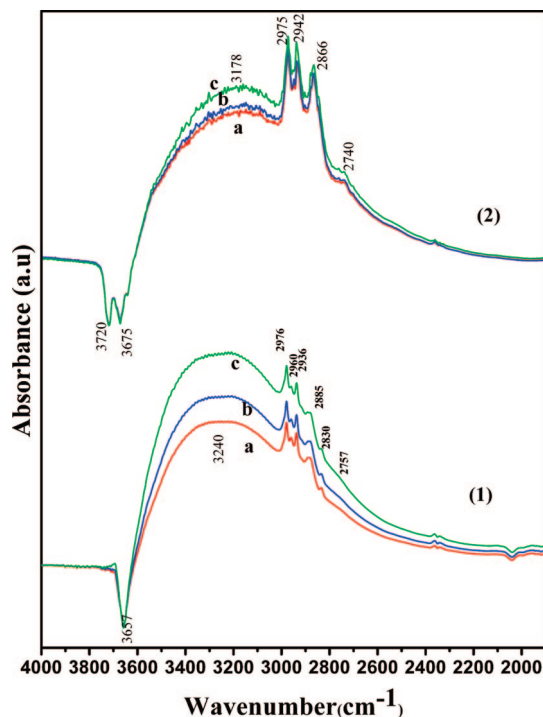


**Figure 9.** *In situ* FTIR spectra, after the UV-irradiation of the ethylene air mixture in the (4000–2000)  $\text{cm}^{-1}$  range, that is, upon evacuation as a function of time on (1) V-doped  $\text{TiO}_2$  for (a) 0 min, (b) 15 min, and (c) 30 min, and on (2) nano  $\text{TiO}_2$  for (a) 0 min, (b) 15 min, and (c) 30 min for the ethylene oxidation upon evacuation in air as a function of time.

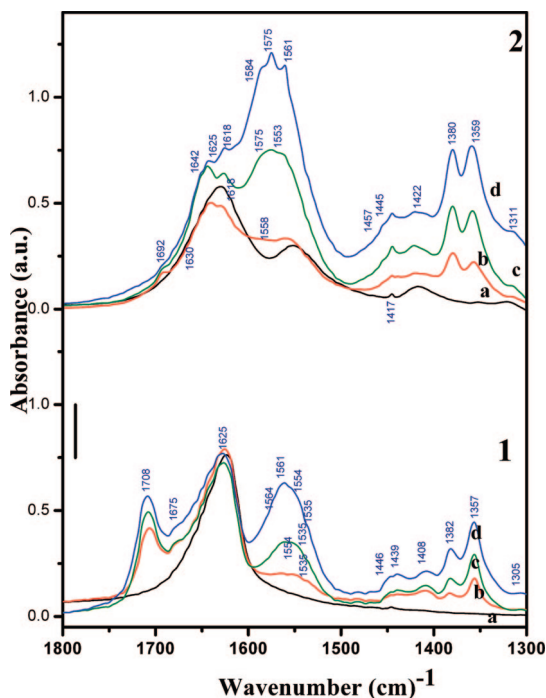


**Figure 8.** *In situ* FT-IR spectra, after the adsorption in the 1800–1300  $\text{cm}^{-1}$  range upon UV irradiation as a function of time, on (1) V-doped  $\text{TiO}_2$  for (a) 0 min, (b) 30 min, (c) 60 min, and (d) 90 min, and (2) on nano  $\text{TiO}_2$  for (a) 0 min, (b) 30 min, (c) 60 min, and (d) 90 min for the ethylene and air mixture.

in intensity with time, revealing that the enolate is very strongly adsorbed in the  $\text{TiO}_2$  surface and the stability increases with time. Again there is a small shoulder at  $1692\text{ cm}^{-1}$  which can be attributed to the  $\nu(\text{C}=\text{O})$  of the unreacted acetaldehyde. The strong peak at  $1575\text{ cm}^{-1}$  and a shoulder at  $1458\text{ cm}^{-1}$  are

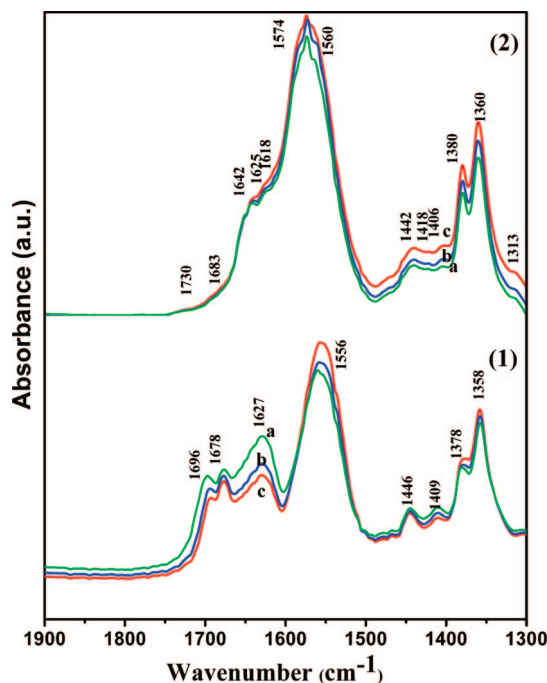


**Figure 10.** *In situ* FTIR spectra, after the UV-irradiation of the ethylene air mixture in the (1900–1300)  $\text{cm}^{-1}$  range, that is, upon evacuation as a function of time on (1) V-doped  $\text{TiO}_2$  for (a) 0 min, (b) 15 min, and (c) 30 min, and on (2) nano  $\text{TiO}_2$  for (a) 0 min, (b) 15 min, and (c) 30 min for the ethylene oxidation upon evacuation in air as a function of time.

assigned to that of the bidentate acetaldehyde adsorbed on the surface.<sup>35</sup> The peak at  $1560\text{ cm}^{-1}$  is for the  $\nu(\text{C}=\text{O})$  of the acetate ions of  $\text{COO}^-$  strongly held on the surface. The peaks at  $1445$  and  $1380\text{ cm}^{-1}$  are due to the  $\nu_{\text{sym}}(\text{COO})$  and  $\delta(\text{CH})$

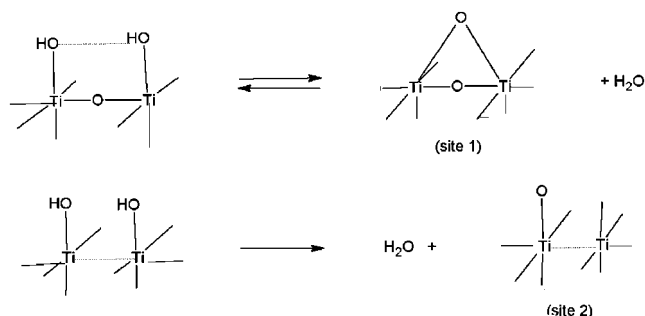


vibrations of bidentate acetate species, respectively. The band at  $1359\text{ cm}^{-1}$  is for the symmetric  $\text{CH}_3$  deformation of the adsorbed acetate ion.

The V-doped  $\text{TiO}_2$  has quite prominent peaks at  $3390$  and  $3210\text{ cm}^{-1}$  which are attributed to the  $\nu\text{ OH-}$  vibrations of the carboxylic acid. Apart from it the bands  $2985$ ,  $2938\text{ cm}^{-1}$  are also for the OH stretch of the acetic acid. The peak at  $2880\text{ cm}^{-1}$  may be due to the acetic acid peak coordinated to the  $\text{V}^{4+}/\text{Ti}^{4+}$  of the V-doped  $\text{TiO}_2$ . The band at  $2760\text{ cm}^{-1}$  is due to the Fermi resonance overtone of the  $-\text{CH}$  stretch for the  $-\text{CHO}$  of the aldehydes. The progressive growth of IR bands centered at  $2360$  and  $2340\text{ cm}^{-1}$  due to  $\nu_3(\text{CO}_2)$  vibrations of carbon dioxide and that at  $1630\text{ cm}^{-1}$  due to the bending vibrations of water confirms the increase in the yield of these products as a function of irradiation time. But in the case of  $\text{Ti}_{0.95}\text{V}_{0.05}\text{O}_2$  compared to that on the  $\text{TiO}_2$  surface, the formation of the  $\text{CO}_2$  with time is quite high. These results indicate that the V-doped  $\text{TiO}_2$  is photocatalytically more active than the nano  $\text{TiO}_2$ . This can also be propagated from the inset of Figure 7, where the intensity of the product  $\text{CO}_2$  (the band at  $2360.44\text{ cm}^{-1}$ ) is plotted against time. It can be easily noticed that the rate of production of  $\text{CO}_2$  for V-doped is much higher than that for nano  $\text{TiO}_2$  and matches well with our photocatalytic activity data. A comparison of IR data presented in Figure 8 reveals the presence of a strong IR band at  $1708\text{ cm}^{-1}$  on the vanadium-doped titania sample (Figure 8, spectra 1) that is missing on the pristine  $\text{TiO}_2$  surface (Figure 8, spectra 2). This band is attributed to the  $\nu(\text{C=O})$  vibrations of acetic acid formed during oxidation of acetaldehyde. Disappearance of this peak upon evacuation suggested its labile nature. Thus, it can be easily inferred that the free and labile acetic acid is produced on the  $\text{Ti}_{0.95}\text{V}_{0.05}\text{O}_2$  surface. Along with this, the peak at  $1439\text{ cm}^{-1}$  (also missing in the  $\text{TiO}_2$  surface) is generally ascribed to the in plane bending vibration of the carboxylic  $-\text{OH}$  group, which also supported the formation of free acetic acid. Similar to that observed on titania, surface acetate species (band at  $1445$  and  $1380\text{ cm}^{-1}$ ) were produced on V-doped  $\text{TiO}_2$ . However, the intensity of these bands, though increased with time, was found to be lower than that observed on the  $\text{TiO}_2$  surface. The peak at  $1675\text{ cm}^{-1}$  is generally assigned to the antisymmetric stretch of the  $-\text{COO}^-$  acid salt, probably due to the salt formation with  $\text{V}^{4+}/\text{Ti}$  sites. The band observed at  $1560\text{ cm}^{-1}$  is for the  $\nu(\text{C=O})$  of the acetate ions of  $\text{COO}^-$  strongly held on the surface. The band at  $1359\text{ cm}^{-1}$  is for the symmetric  $\text{CH}_3$  deformation of the adsorbed acetate ion. The band at  $1408\text{ cm}^{-1}$  is due to the  $\nu_{\text{sym}}(\text{C-O-M})$  vibrations of the acetate salt. The marked absence of the peaks at  $1575$  and  $1584\text{ cm}^{-1}$  and that at  $1642\text{ cm}^{-1}$  on the V-doped surface (Figure 8, spectra 1) suggests that the aldehydic species and the enolates are not as stabilized as they are on a nano titania surface, and they are converted to the acetate species which are present in both free and adsorbed forms, thereby facilitating the yield and the rate of formation of the  $\text{CO}_2$ . Again this point will become apparent once we inspect the evacuation effect as described in the next portion. Another point that is worth mentioning here is that the relative intensities of the IR bands at  $1380$  and  $1357\text{ cm}^{-1}$  on the two samples are different. On a nano titania sample the intensities of both these peaks increase equally with time, whereas in the case of a V-doped surface, the  $1382\text{ cm}^{-1}$  band is not growing as strongly as the other. The  $1382\text{ cm}^{-1}$  band is also assigned for the bidentate formate species,<sup>36</sup> attached to the Ti surface,  $\text{HCOO-Ti}$  type, which may be formed due to the stabilization of the enolate and formation of the  $\text{HCHO}$  and subsequent oxidation to  $\text{HCOOH}$  in that route, as explained in the reaction

mechanism scheme presented later. This explains the fact that in the V-doped  $\text{TiO}_2$  the formate produced from the enolate route is not stabilized but in the  $\text{TiO}_2$  surface this is the case.

It is quite relevant here to take a view of the negative bands in the hydroxyl region. Figure 7a reveals at least three differently coordinated  $-\text{OH}$  groups at the  $\text{TiO}_2$  surface, appearing at the frequencies of  $\sim 3715$ ,  $3657$ , and  $3640\text{ cm}^{-1}$ , the presence of which have been reported earlier.<sup>37</sup> The negative absorbance values for all these  $-(\text{OH})$  bands in Figure 7a (peaks pointing downward) indicate the involvement of different  $\text{Ti-OH}$  groups in the formation of corresponding  $\text{CH}_3-\text{CH}_2-\text{O}-$  groups on interaction with the adsorbed  $\text{CH}_2=\text{CH}_2$  on the surface irrespective of the coordination environment. There is a clear depletion of these  $\text{Ti-OH}$  sites with time as we get more and more negative bands. But for the V-doped  $\text{TiO}_2$  surface we get basically two differently coordinated  $-\text{OH}$  groups appearing at  $3715\text{ cm}^{-1}$  and another at  $3657\text{ cm}^{-1}$ . The negative peak of  $3715\text{ cm}^{-1}$  is quite a weak one and is almost absent here. The earlier studies on the surface hydroxyl species of the anatase titania do propagate that there are two different types of  $-\text{OH}$  groups linked with the Ti at the two different sites.<sup>38,39</sup> Sites I and II are as follows:



Site 1 has hydroxyl groups, which for anatase are at  $3655\text{ cm}^{-1}$ , whereas for site 2 the hydroxyl groups of anatase titania have a band at  $3715\text{ cm}^{-1}$ . The site 1 hydroxyl groups are very labile for dehydroxylation. But here, for the V-doping, the site 2  $-\text{OH}$  groups are more labile and can be used to lose the lattice electron and thereby reduce  $\text{V}^{5+}$  to  $\text{V}^{4+}$ , as inferred in our earlier publication.<sup>19,20,25</sup> So, in the case of a V-doped  $\text{TiO}_2$  sample, the IR band at  $3715\text{ cm}^{-1}$  due to an isolated hydroxyl group is utilized for the reduction of  $\text{V}^{5+}$  to  $\text{V}^{4+}$ , as has been discussed earlier, while the increasing intensity of the negative IR band at  $3657\text{ cm}^{-1}$  suggested its participation in the formation of  $\text{CH}_3-\text{CH}_2-\text{O}^-$  species on the V- $\text{TiO}_2$  surface.

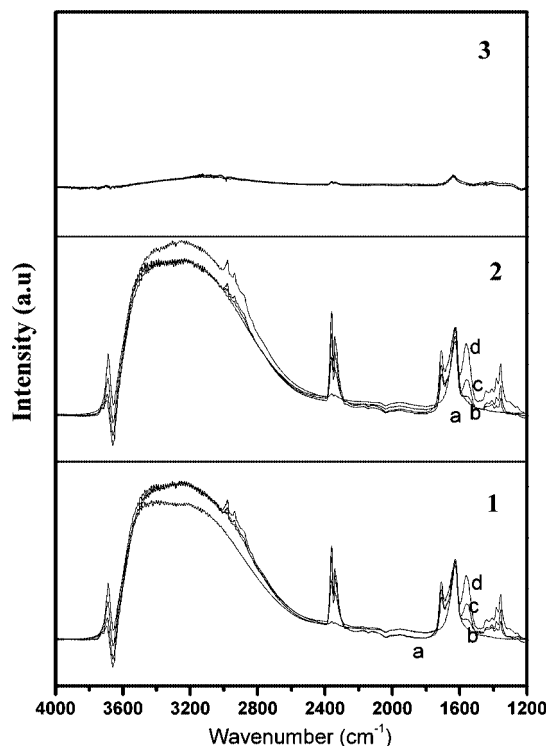
**(c) Effects of Evacuation after Irradiation on an Ethylene and Air Mixture Subsequent to Adsorption over Nano  $\text{TiO}_2$  and V-Doped  $\text{TiO}_2$ .** The comparative effect of evacuation after 90 min of irradiation for 5, 15, and 30 min is presented in Figures 9 and 10. IR bands at  $2975$ ,  $2942$ , and  $2866\text{ cm}^{-1}$  associated with the ethoxy species on a titania surface were still present even after 30 min of evacuation. The increased intensity of the IR band at  $2942\text{ cm}^{-1}$  could also be attributed to the contribution of adsorbed ethylene and the acetate species absorbing in this region. It can be inferred from the shape and the intensity of these bands that they are strongly adsorbed ethoxy groups which did not undergo the reaction, lowering the yield of product on the  $\text{TiO}_2$  surface. Another prominent feature in Figure 9 is the lowering of the intensity of the broad peak in the  $3500-3100\text{ cm}^{-1}$  region on both surfaces, and the effect was more pronounced on V-doped titania. Also there is a shoulder appearing at  $2740\text{ cm}^{-1}$  which can be ascertained to



the Fermi resonance overtone of the -CH stretch for the -CHO of the aldehydes, which signifies the stability of the strongly adsorbed aldehydic species. On the lower frequency side, the shoulder at  $1683\text{ cm}^{-1}$  [ $\nu(\text{C}=\text{O})$ ] for the stabilized acetaldehyde with the strong peak at  $1574\text{ cm}^{-1}$  for the bidentate acetaldehyde confirms the stable adsorbed and unreacted acetaldehyde on the surface of  $\text{TiO}_2$ . Even after evacuation, the presence of vibrational bands at  $1642\text{ cm}^{-1}$  along with the weak shoulder at  $1618\text{ cm}^{-1}$  [ $\nu(\text{C}=\text{C})$  vibration of enolate] indicated the stability of enolate on the  $\text{TiO}_2$  surface. The small shoulders at  $1445\text{ cm}^{-1}$  and the peak at  $1380\text{ cm}^{-1}$  are due to the  $\nu_{\text{as}}(\text{COO})$  and  $\delta(\text{CH})$  of bidentate acetate species. The prominence of the  $1380\text{ cm}^{-1}$  peak on titania even after the evacuation signifies the stabilization of the bidentate formate species also. The band at  $1359\text{ cm}^{-1}$  is for the symmetric  $\text{CH}_3$  deformation of the adsorbed acetate ion, signifying the stability of the acetate ions here also.

The prominent bands seen on the V- $\text{TiO}_2$  surface (Figure 9) at  $2970$  and  $2936\text{ cm}^{-1}$  are typical of  $\nu_{\text{as}}(\text{COO})^- + \delta(\text{CH})$  combination bands of mono- and bidentate acetate species, and the bands at  $2885$  and  $2826\text{ cm}^{-1}$  are assigned to corresponding  $\nu(\text{CH})$  vibrations. The shoulder band at  $2730\text{ cm}^{-1}$  may be associated with the  $2\delta(\text{CH})$  vibrations of acetate species. There is a marked difference in the intensity and the structure of the bands in the  $1900\text{--}1300\text{ cm}^{-1}$  region between the two samples. The peak at  $1692\text{ cm}^{-1}$  is due to the  $\nu(\text{C}=\text{O})$  for the adsorbed acetaldehyde. The peak at  $1675\text{ cm}^{-1}$  is generally assigned to the antisymmetric stretch of the  $-\text{COO}^-$  acids salt, probably due to the salt formation with  $\text{V}^{4+}/\text{Ti}$  sites, suggesting that the acetate ions are more stabilized on the V- $\text{TiO}_2$  surface. That recorded at  $1560\text{ cm}^{-1}$  is for the  $\nu(>\text{C}=\text{O})$  of the acetate ions of  $\text{COO}^-$  strongly held on the surface. The presence of IR bands at  $1445$  [ $\nu_{\text{as}}(\text{COO})$ ],  $1380$  [ $\delta(\text{CH})$ ],  $1408$  [ $\nu(-\text{C}-\text{O}-\text{M})$ ], and  $1359$  [ $\delta(\text{CH}_3)_{\text{sym}}$ ]  $\text{cm}^{-1}$  after evacuation suggested the stability of acetate species on the V- $\text{TiO}_2$  surface; however, there is a marked difference in the stability in the adsorbed intermediate species present on these two surfaces. Thus, on V-doped  $\text{TiO}_2$ , the aldehydes are predominantly stabilized and are transformed into acetates/acetate salts, which are then held strongly on the surface, whereas on the  $\text{TiO}_2$  surface the enolate form is more stabilized, which on subsequent oxidation gives rise to aldehydes, which are very strongly adsorbed and yield less amount of acetates upon further oxidation, thereby lowering the amount of  $\text{CO}_2$  produced. Also, formation of the formaldehyde from the enolates species on a  $\text{TiO}_2$  surface and its transformation to formates further reduces the amount of acetates. This is more vividly described in the mechanistic scheme.

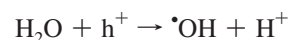
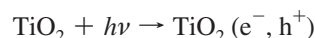
**(d) Effects of Irradiation on Ethylene and Air Mixtures Subsequent to Adsorption over Nano  $\text{TiO}_2$  and V-Doped  $\text{TiO}_2$  under the Visible Irradiation.** Figure 11 shows comparative IR results on photocatalytic oxidation of ethylene over V-doped  $\text{TiO}_2$  and nano  $\text{TiO}_2$  when carried out under visible light irradiation as a function of time (0, 30, 60, and 90 min). Compared to nano titania, the V-doped sample is found to be quite active under the visible irradiation and the absorption bands produced are similar to that observed during UV irradiation (Figures 7 and 8). From these results it can be inferred that under both the UV and the visible irradiation the photocatalytic oxidation of ethylene over V-doped  $\text{TiO}_2$  may follow the similar pathways. Poor absorption of nano titania in the visible region makes it inactive for the ethylene oxidation under visible irradiation. The photocatalytic oxida-

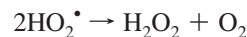
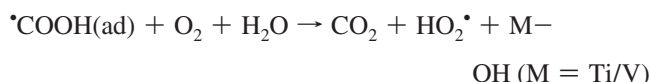
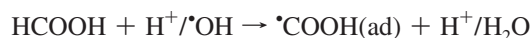
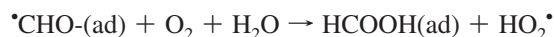
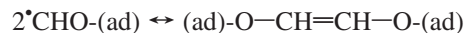
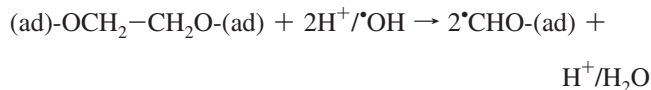
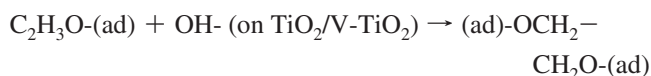
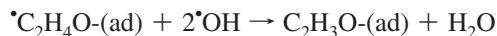
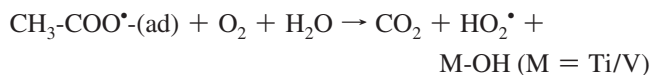
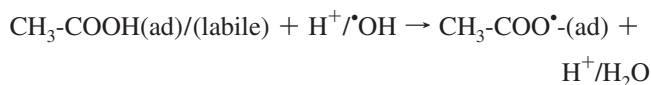
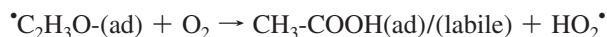
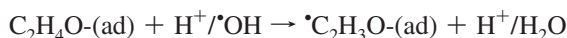
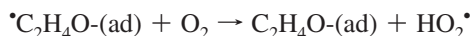
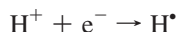
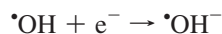


**Figure 11.** *In situ* FTIR profiles for comparison between UV and visible irradiation of V-doped  $\text{TiO}_2$  and nano  $\text{TiO}_2$ : (1) V-doped  $\text{TiO}_2$  under UV-radiation; (2) V-doped  $\text{TiO}_2$  under UV-radiation; and (3) nano  $\text{TiO}_2$  under Vis-radiation for the ethylene oxidation upon adsorption in air as a function of time from  $4000$  to  $1200\text{ cm}^{-1}$ . In each of the above FTIR profiles, (a) 0 min, (b) 30 min, (c) 60 min, and (d) 90 min, respectively.

tion experiment carried out under the visible irradiation has resulted in a temperature rise of up to  $\sim 65^\circ\text{C}$ . Again when the reactions were carried out at this temperature without any irradiation, they did not result in any intermediate or product formation, respectively, for both the catalysts. Thus, the results obtained during visible irradiation can be attributed to the photocatalytic effect only.

**3.5. Plausible Mechanism for the Photocatalytic Oxidation of  $\text{C}_2\text{H}_4$  on the  $\text{TiO}_2$  and the V-Doped  $\text{TiO}_2$  Surfaces.** The mechanistic study by the *in situ* FT-IR for the aqueous phase reactions on the  $\text{TiO}_2$  surface has been well documented by Nakato et al., where they propose that the oxygen photoevolution reaction is initiated by the nucleophilic attack of an  $\text{H}_2\text{O}$  molecule on a surface trapped hole.<sup>39,40</sup> On the other hand, the molecular mechanism of oxygen photoevolution has been assumed for a longer period and they proclaim the  $\text{OH}^{\bullet-}$  (produced from initial hole trapping in the  $[\text{Ti}-\text{OH}]$  to produce  $[\text{Ti}^{\bullet}\text{OH}]^+$ ) to be the key intermediate for the photocatalytic degradation of organics on the  $\text{TiO}_2$  surface.<sup>9-11,17,20,21,36,41-43</sup> From the previous discussion and the literature on oxidation of the ethylene molecule or the alkenes, we propose the mechanism for oxidation of the  $\text{C}_2\text{H}_4$  on  $\text{TiO}_2$  and the V-doped  $\text{TiO}_2$  surface in the following way.



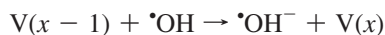
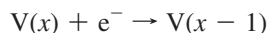


The salient features of the above reaction mechanism are portrayed in Scheme I given below. From the above discussion and the reaction mechanism it is quite evident that on pristine  $\text{TiO}_2$  anatase surface the species which are adsorbed and stable are ethoxy, enolates, and subsequently the aldehydes. The formation of the formates in the  $\text{TiO}_2$  surface also validates the occurrence of step 1 primarily for the pristine anatase  $\text{TiO}_2$  surface. The subsequent formation and the stabilization of the acetates in the step 2 channel is low as compared to that of the V-doped  $\text{TiO}_2$ . However, in the V-doped  $\text{TiO}_2$  surface the most stable species adsorbed are the acetates or the acetate salts. So going by the stable adsorbed intermediates, the ethoxy species are transformed to aldehyde and subsequently to the acetates following the step 2 channel.

Now on doping vanadium in the 4+ state in the  $\text{TiO}_2$  crystal lattice, it is quite evident from our XPS discussion that the  $\text{Ti}^{4+}$  state is shifted to the higher binding energy side, thereby producing the  $\text{Ti} (4+\delta)$  state. So the out of these nucleophilic intermediates produced as intermediates the  $\text{CH}_3\text{COO}^-$  is a stronger nucleophile than the enolates or the aldehydic species. On doping  $\text{V}^{4+}$  in the  $\text{TiO}_2$  as Ti is having a  $\text{Ti} (4+\delta)$  as compared to the Ti in  $\text{TiO}_2$  the acetate will get adsorbed more strongly here, and the enolates and the aldehydic species in the  $\text{TiO}_2$  pristine surface. The substitution of the metal ion in the lattice sites of the host matrix creates definite Lewis acid sites and the Bronsted acid sites at the molecular level.<sup>44</sup> Thus, on doping the  $\text{V}^{4+}$  in the  $\text{Ti}^{4+}$  sites, the  $\text{Ti}^{(4+\delta)}$  acts as stronger Lewis acid sites; thereby, attachment of the stronger nucleophiles is facilitated here.

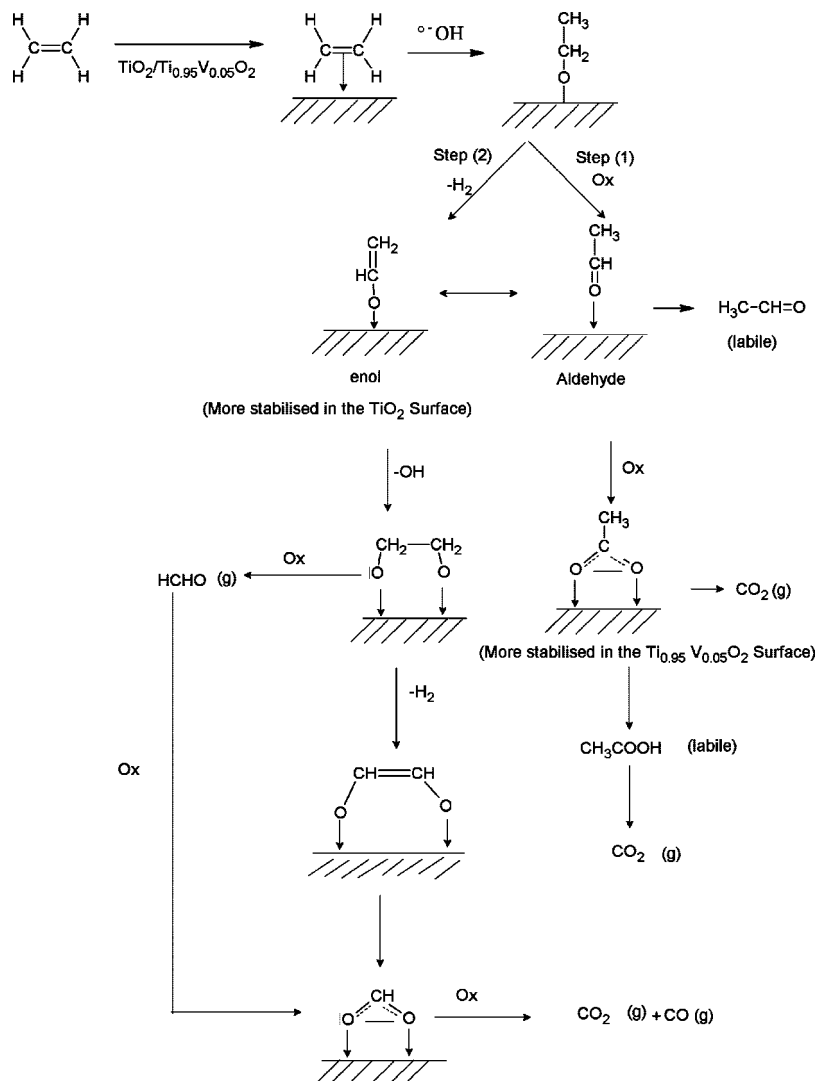
Apart from this, the doped  $\text{V}(4+)$  can effectively act in this way to promote the formation of the  $\cdot\text{OH}^-$  radical ion in the following way.

## SCHEME I:



This formation of the hydroxyl anionic radical by the doped  $V(4+)$  appends to the total formation of this radical essentially required in the oxidation mechanism, thereby increasing the yield of  $CO_2$ .

surface, leading to formation of formates along with the acetates. The aldehydic species are also far more stabilized on the nano  $TiO_2$  surface as compared to vanadium-doped  $TiO_2$ , thereby lowering the formation of the acetates and later the formation of  $CO_2$ . In the vanadium-doped  $TiO_2$ , on the other hand, the acetates are far more stabilized. The formation of the acetates is through the initial stabilization of the acetaldehyde rather than its enol tautomer. The formation of the labile acetic acid, the adsorbed acetates, and the adsorbed acetate  $-M$  salts leads to easier oxidation of them to provide a higher yield of  $CO_2$ . The Ti of the  $Ti_{0.95}V_{0.05}O_2$  is in the Ti  $(4+\delta)$  state as compared to



## 4. Conclusion

The vanadium is doped in the crystal lattice of  $TiO_2$ . The doped vanadium is present in the  $V^{4+}$  state. The vanadium-doped titania is photocatalytically more active than nano titania. The photo-oxidation of ethylene leads to complete oxidation products of  $CO_2$  and  $H_2O$ . On adsorption the V-doped titania acts as a better photocatalyst because of the fact that it has more chemisorbed hydroxyl species. Again during the calcination process the isolated hydroxyl groups represented by the IR band at  $3715\text{ cm}^{-1}$  are used for the reduction of  $V^{5+}$  to  $V^{4+}$ . The ethylene decomposition occurs via formation of ethoxy, transformed to acetaldehyde or enolates, subsequently to acetates, and then to  $CO_2$ . The enolates are more stabilized on the  $TiO_2$

that of Ti of the nano  $TiO_2$ , due to the doped vanadium in the  $4+$  state. This thereby helps in the adsorption of the stronger nucleophile among all the intermediate nucleophiles formed, that is the acetate in the free and the adsorbed and the metal acetates forms, thereby increasing the yield of the  $CO_2$ .

**Acknowledgment.** The authors acknowledge Dr. D. Das for his deep interest in the work.

## References and Notes

- (1) Weckhuysen, B. M.; Keller, D. E. *Catal. Today* **2003**, 78, 25.
- (2) Berty, J. M. In *Applied Industrial Catalysis*; Leach, B. E., Ed.; Academic Press: New York, 1983; Vol. I, p 207.
- (3) Smidt, J.; Hafner, W.; Jira, R.; Sedlmeier, R.; Siebner, R.; Ruttinger, R.; Kojer, H. *Angew. Chem.* **1959**, 71, 176.

- (4) Chen, X.; Mao, S. S. *Chem. Rev.* **2007**, *107*, 2891–2959.
- (5) Anpo, M.; Ichihashi, Y.; Takeuchi, M.; Yamashita, H. *Res. Chem. Intermed.* **1998**, *24*, 143.
- (6) Zhao, G.; Kozuka, H.; Lin, H.; Yoko, T. *Thin Solid Films* **1999**, *339*, 123.
- (7) Choi, W.; Termin, A.; Hoffmann, M. R. *J. Phys. Chem.* **1994**, *98*, 13669.
- (8) Choi, W.; Termin, A.; Hoffmann, M. R. *Angew. Chem., Int. Ed. Engl.* **1994**, *33*, 1091.
- (9) Mori, K.; Miyamoto, A.; Murakami, Y. *J. Phys. Chem.* **1984**, *88*, 2741.
- (10) Escibano, V. S.; Busca, G.; Lorenzelli, V. *J. Phys. Chem.* **1991**, *95*, 5541–5545.
- (11) Escibano, V. S.; Busca, G.; Lorenzelli, V. *J. Phys. Chem.* **1990**, *94*, 8939–8945.
- (12) Busca, G.; Cavani, F.; Trifiro, F. *J. Catal.* **1987**, *106*, 471.
- (13) Busca, G.; Ramis, G.; Lorenzelli, V. *J. Mol. Catal.* **1989**, *55*, 1.
- (14) Bum, G.; Ramis, G.; Lorenzelli, V. In *New developments in selective oxidation*; Trifiro, F., Centi, G., Eds.; Elsevier: Amsterdam, 1990; p 825.
- (15) Busca, G.; Elmi, S. A.; Forzatti, P. *J. Phys. Chem.* **1987**, *91*, 5263–5269.
- (16) Jeffrey, R. S.; Brownson, M.; Isabel, T.-T.; Anderson, M. A. *Chem. Mater.* **2005**, *17*, 6304–6310.
- (17) Martin, T. S.; Morrison, C. L.; Hoffmen, M. R. *J. Phys. Chem.* **1994**, *98*, 13695–13704.
- (18) Escibano, V. S.; Busca, G.; Lorenzelli, V. *J. Phys. Chem.* **1990**, *94*, 8945–8950.
- (19) Bhattacharyya, K.; Varma, S.; Kishore, K.; Gupta, N. M. *Res. Chem. Intermed.* **2006**, *32*, 17–30.
- (20) Bhattacharyya, K.; Varma, S.; Tripathi, A. K.; Bharadwaj, S. R.; Tyagi, A. K. *J. Phys. Chem. C* **2008**, *112*, 19102.
- (21) Klosek, S.; Raftery, D. *J. Phys. Chem. B* **2001**, *105*, 2815–2819.
- (22) Trifiro, F. *Catal. Today* **1998**, *41*, 21.
- (23) Herrmann, J.-M.; Disdier, J.; Deo, G.; Wachs, I. E. *J. Chem. Soc., Faraday Trans.* **1997**, *93*, 1655.
- (24) Arnett, A. L.; Crawford, B. L. *J. Chem. Phys.* **1953**, *18*, 118.
- (25) Duncan, J. L.; McKean, D. C.; Mallison, P. D. *J. Mol. Spectrosc.* **1973**, *45*, 221.
- (26) Knippers, W.; Helvoort, K. Van.; Stolte, S.; Reuss, J. *Chem. Phys.* **1985**, *98*, 126.
- (27) Busca, G.; Elmi, A. S.; Forzatti, P. *J. Phys. Chem.* **1987**, *91*, 5263.
- (28) Owen, N. L.; Sheppard, N. *Trans. Faraday Soc.* **1964**, *60*, 634.
- (29) Sullivan, J. F.; Dickson, T. J.; Durig, J. R. *Spectrochim. Acta* **1986**, *42A*, 113.
- (30) Busca, G.; Zerla, T.; Lorenzelli, V.; Girelli, A. *J. Catal.* **1984**, *88*, 125.
- (31) Goodsel, A. J. *J. Catal.* **1973**, *30*, 175–186.
- (32) Bezrodna, T.; Puchkovska, G.; Shymanovska, V.; Baran, J.; Ratajczak, H. *J. Mol. Struct.* **2004**, *700*, 175–181.
- (33) Bezrodna, T.; Puchkovska, G.; Shymanovska, V.; Chashechnikova, I.; Khalyavka, T.; Baran, J. *Appl. Surf. Sci.* **2003**, *214*, 222.
- (34) Shurvell, H. F. In *Handbook of Vibrational Spectroscopy*; Chalmers, J. M., Griffith, P., Eds.; Wiley: New York, NY, 2002; p 1086.
- (35) Martin, C.; Martin, I.; Rives, V. *J. Chem. Soc., Faraday Trans.* **1993**, *89*, 4131–4135.
- (36) Bhattacharyya, K.; Varma, S.; Kumar, D.; Tripathi, A. K.; Gupta, N. M. *J. Nanosci. Nanotechnol.* **2005**, *5*, 797.
- (37) Busca, G.; Saussey, H.; Saur, O.; La valley, J. C.; Lorenzelli, V. *Appl. Catal.* **1985**, *14*, 245.
- (38) Primet, M.; Picha, P.; Matheu, M.-V. *J. Phys. Chem.* **1971**, *75*, 1216–1220.
- (39) Nakamura, R.; Nakato, Y. *J. Am. Chem. Soc.* **2004**, *126*, 1290.
- (40) Nakamura, R.; Okamura, T.; Naomichi, O.; Imanashi, A.; Nakato, Y. *J. Am. Chem. Soc.* **2005**, *127*, 12975.
- (41) Ollis, D. S.; AL-Ekabi, H. *Photocatalytic Purification and Treatment of Water and Air*; Elsevier: Amsterdam, 1992.
- (42) Fujishima, A.; Rao, T. N.; Tyrk, D. A. *J. Photochem. Photobiol. C: Photochem. Rev.* **2000**, *1*, 1–21.
- (43) Hoffmann, M. R.; Martin, S. T.; Choi, W. Y.; Bahemann, D. W. *Chem. Rev.* **1995**, *95*, 735.
- (44) Notari, B.; Willey, R. J.; Panizzab, M.; Busca, G. *Catal. Today* **2006**, *116*, 99–110.